Eur. Phys. J. B **11**, 593–608 (1999)

THE EUROPEAN PHYSICAL JOURNAL B

EDP Sciences

Undulation instability of lamellar phases under shear: A mechanism for onion formation?

A.G. Zilman and R. Granek[a]

Department of Materials and Interfaces, Weizmann Institute of Science, Rehovot 76100, Israel

Received 15 April 1998 and Received in final form 4 March 1999

Abstract. We consider a lamellar phase of bilayer membranes held between two parallel plates and subject to a steady shear. Accounting for the coupling with the shear flow of the short wavelength undulation modes that are responsible for the membrane excess area, we argue that the flow generates an effective force which acts to reduce the excess area. From the viewpoint of the macroscopic lamellar whose geometric dimensions are fixed, this force translates into an effective lateral pressure. At low shear rates $\dot{\gamma}$ this pressure is balanced by the elastic restoring forces of the lamellar. Above a critical shear rate $\dot{\gamma}_{\rm c} \sim d^{-5/2}D^{-1/2}$, where d is the interlayer distance and D is the gap spacing, the lamellar buckles into a harmonic shape modulation, and we predict its wavelength $\lambda_{\rm c}$ and amplitude $U_{\rm o}$. We show that our model is isomorphic to a dilative strain, which is known to induce a similar buckling (undulation) instability. Indeed, at threshold the wavelength is $\lambda_{\rm c} \sim \sqrt{Dd}$ and is identical in both cases. Using a non-linear analysis, we discuss how the wavelength and amplitude vary with shear rate away from the threshold. For $\dot{\gamma} \gg \dot{\gamma}_{\rm c}$ we find $\lambda_{\rm c} \sim \dot{\gamma}^{-1/3}$ and $U_{\rm o} \sim \dot{\gamma}^{2/3}$. We then focus on the coupling of the buckling modulation itself with the flow, and obtain a criterion for the limit of its stability. Motivated by experiments of D. Roux and coworkers, we assume that at this limit of stability the lamellar breakups into "onion"-like, multilamellar, vesicles. The critical shear rate $\dot{\gamma}^*$ for the formation of onions is predicted to scale as $\dot{\gamma}^* \sim \dot{\gamma}_{\rm c} \sim d^{-5/2}D^{-1/2}$. The scaling with d is consistent with available experimental data.

PACS. 64.70.Md Transitions in liquid crystals – 61.30.Jf Defects in liquid crystals – 68.10.Et Interface elasticity, viscosity, and viscoelasticity

1 Introduction

During recent decades there has been a lot of advance in understanding the equilibrium phase diagrams of many complex fluid systems, and, in particular, those of self-assembly systems [1–3]. Even for systems were more work needs to be done, such as those involving strong electrostatic interactions, the procedure for comparing the stability of different phases relies on well established thermodynamic concepts. The uncertainty in understanding and in predicting various observable lies mainly at the level of modeling and approximations made in calculating system free-energies.

Non-equilibrium transitions, such as those obtained under steady shear, still await major breakthroughs in understanding. Here, we would like to distinguish between two classes: (i) One in which the shear flow selects a particular phase which otherwise exists in equilibrium, and (ii) the other in which the shear induces a state which is either metastable or unstable in equilibrium. For the first class, an extensive amount of theoretical work has been performed in the past decade, following the pioneering work of Onuki [4] and of Fredrickson [5]. Cates and coworkers [6] have considered in particular self-assembly systems under shear flow and demonstrated how the coupling between the order parameter and the shear can account for a shift in the critical transition controlling parameter (*e.g.*, temperature, density, etc.). These studies give a qualitative explanation for the observed variety of shear induced transitions in surfactant and diblock copolymer systems, for example, the shear induced sponge (L_3) to lamellar (L_α) transition [7]. More recent theoretical work concerns with the possibility of two phase coexistence under shear flow [8,9], which has been observed experimentally in worm-like micellar systems [9]. However, when the shear induced state is not related to an existing equilibrium phase [10], the reason for its appearance is less clear and should probably be based on a specific instability mechanism [11]. While this viewpoint is somewhat discouraging since it prevents the formulation of a general theory, it may explain why a large variety of states – much more than those existing in equilibrium – are often obtained under shear.

In equilibrium, surfactants in solutions self-assemble in a variety of building block structures, one of which is a bilayer membrane [2]. In the lamellar phase [12], which has the symmetry of smectic-A liquid crystals, the membranes

[a] e-mail: cpgranek@weizmann.weizmann.ac.il

are arranged in a periodic stack with repeat distance d. The equilibrium properties of dilute lamellar phases of uncharged, semi-flexible, membranes, are well understood. A key quantity is the so-called Helfrich-Servuss patch size $\xi_\parallel$, the distance between consecutive intermembrane collisions. It is related to the single membrane bending modulus κ and to the interlayer spacing d according to $\xi_\parallel \sim (\kappa/k_{\rm B}T)^{1/2}d$ ($\kappa \sim 1-5\ k_{\rm B}T$ for typical systems). On lateral lengthscales shorter than $\xi_\parallel$ the membrane behave as if it was isolated. On lateral lengthscales much longer than $\xi_\parallel$, the membrane collides with neighboring membranes, giving rise to an effective entropic repulsion. The collective membrane fluctuations at such long wavelengths are well described by the usual smectic-A elasticity [13], in which both bending and compression moduli are related to the single membrane bending modulus.

Much less is understood about the non-Newtonian behavior of these lamellar phases under shear. In the experiments performed by Roux and co-workers [10,14–17] it has been found that under relatively low shear rates (typically $\sim 1\ {\rm s}^{-1}$ for most systems) lamellar phases transform into a "phase" of spherulites, *i.e.*, multilamellar, onion-like, vesicles. The local order of this phase is thus lamellar, but not anymore the long range order. A detailed "orientation phase diagram" has been obtained, showing the variation of the critical shear rate $\dot\gamma^*$ for the formation of onions as the interlayer distance d is changing. The onion phase transforms back into a well ordered lamellar phase at a higher critical shear rate, which we do not discuss here. The phase diagram appears essentially universal, with small quantitative changes from one system to another. Recent experiments show that onions are also formed in lamellar-colloidal mixtures, in which case they encapsulate the colloidal particles [18].

The mechanism of onion formation remains however unclear to a large extent. Roux and co-workers have conjectured [10] that the transition to onions is triggered by a buckling (or undulation) instability. This occurs, as they suggest on the basis of theoretical work of Oswald, Kleman and coworkers [19], because in the experiment the gap between the two sliding surface is not uniform. In equilibrium this spatial variation in the gap is accommodated by the existence of dislocations which permit a change in the local number of layers. These dislocations are able to move with the mean flow at sufficiently low shear rates. However, when the shear rate is too high the dislocations cannot follow the flow [19] and this gives rise to an effective dilative (or compressive) strain perpendicular to the layers. This dilatation is then suggested to trigger the well known undulation (buckling) instability [13,20], which is also found in controlled dilatation experiments (in the absence of flow). Since the buckling pattern cannot easily flow, it may not sustain a large shear, and so its evolution into an onion state is quite natural; no quantitative criterion for this transition has been offered however by Roux and co-workers.

While this idea that a buckling instability triggers the formation of onions is very appealing, the mechanism that has been suggested for its appearance in the first place is not universal, even if plausible. In particular, it implies that some of the transition characteristics may vary from one apparatus to another, and possibly even under different sample preparations giving rise to different type of defects. It is therefore interesting to explore also the possibility that a lamellar phase will buckle under shear even at uniform gap conditions. In this paper we present a novel mechanism for such an instability that is inherent to lyotropic lamellar phases. Our mechanism involves the coupling of the short wavelength membrane undulations to the flow. These short wavelength undulations are those responsible for the (so-called) membrane excess area, and we argue that these undulations are suppressed by the flow [21]. Indirect observations for such an effect have been recently reported [22]. It should be noted that this coupling is very weak at the shear rates of interest. However, it is sufficient to promote transmission of membrane area from "excess" to "projected". The shear effect is introduced as an effective lateral pressure in the coarse grained lamellar free-energy, which induces buckling of the whole phase above a certain critical value. We show that our free-energy is, in fact, isomorphic to the elastic free-energy change under dilatation, with the effective pressure acting as the dilatation parameter. We also provide a criterion for the formation of onions from the buckling array. This allows us to predict, with the help of the asymptotic results for the buckling wavelength and amplitude, the critical shear rate for onion formation. Interestingly, our approach bears some similarity to the study of Williams and MacKintosh [23] of diblock copolymer smectic-A phase under shear. Here, it was suggested that the shear tilts (and thus stretches) the polymers, which causes the layer thickness to diminish giving rise to an effective dilatation.

The undulation (or buckling) instability of smectic-A phases under dilatation or external field is a well known phenomena [13,24,25]. From the theoretical viewpoint the main approach has been a linear stability analysis of the elastic Landau-de-Gennes free-energy. Other works [26] have shown that if topological transformations are allowed, focal conic domains prevail at a slightly larger dilatation than the critical one. More recently, non-linear analysis of the buckling profile has been performed by Singer for large dilatation [20], keeping, in contrast, a fixed topology (*i.e.*, not allowing the formation of focal conics). This is relevant to situations where the energy barrier to obtain focal conics is too high so that the transition is kinetically suppressed. Analytical results for the buckling amplitude and wavelength have not been obtained however. Our non-linear analysis stems from the calculation of Singer and allows us to find asymptotic expressions for the buckling wavelength and amplitude at small and large shear rates (effective pressures). The dynamics of the undulation instability has also been recently addressed [27]. This issue will not be considered here, because the undulation instability is expected to evolve much faster than the subsequent transition to onions, so that an "equilibrium" analysis of the instability is useful.

Our paper is constructed as follows. In Section 2 we discuss the coupling of the short wavelength membrane

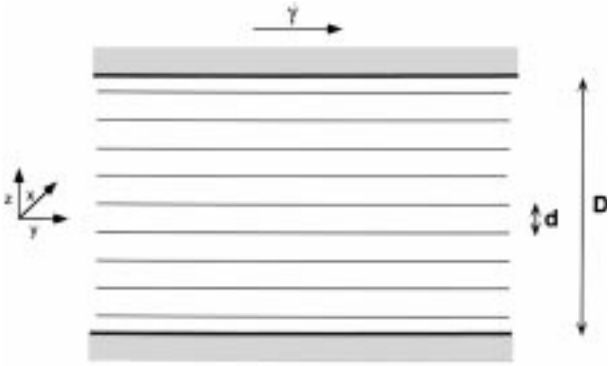

Fig. 1. A lamellar phase held in a parallel plate shear cell (schematic illustration). The small number of layers is not realistic.

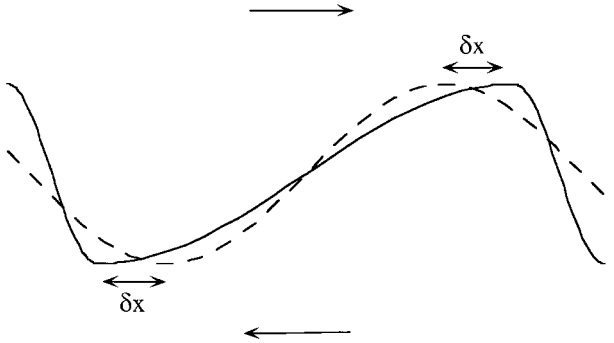

Fig. 2. A single membrane undulation mode, $h(x) = h_q \sin(qx)$ (dashed line), which is perturbed by the shear flow (solid line). The extent of the deformation δx is determined by a force balance, see Section 2.

thermal undulations with the shear flow and describe how the effect of shear flow can be replaced by an effective lateral pressure. Combining this pressure with the lamellar elastic free-energy, we construct in Section 3 a virtual free-energy for an oriented lamellar phase under shear. In Section 4.1 we repeat the familiar linear analysis of this free-energy showing the onset of a buckling (undulation) instability. Our results are extended in Section 4.2 beyond the linear analysis by obtaining an exact integral expression for the minimum free-energy. The latter is analyzed analytically both in the small shear rate (or dilatation) and large shear rate regimes, to obtain the preferred wavelength of the instability as a function of shear rate. In Section 4.3 we compare the stability of the square lattice and stripe modulations. In Section 5 we then derive a criterion for the stability limit of the buckling modulation itself due to its coupling with the flow, above which it is unstable. Assuming that at this limit of stability it breakups into onions, we compare our predictions to existing experimental data. We discuss our main assumptions and conclude in Sections 6, 7.

2 A single membrane under shear flow

2.1 Microscopic picture – general considerations

We consider an ideal rheometer composed of two parallel smooth walls (even though many of the actual experiments have been done in a couette cell). A lamellar phase is sandwiched in the gap and the top wall is moved at a constant velocity, making a constant shear rate (velocity gradient), see Figure 1. We assume that the lamellar planes become oriented parallel to the walls ("c" orientation), as usually found in experiment [10]. We denote by z the axis perpendicular to the walls (the ∇v direction), y be the axis parallel to the flow (v direction) and x be perpendicular to both.

We assume a perfect lamellar order, *i.e.*, that no defects are present. For simplicity, we also freeze in all *long* wavelength ($\lambda \gg \xi_\parallel$) thermal fluctuations of the lamellar. These can be added in a more refined calculation. We shall thus focus on the interaction with the shear flow of the short wavelength undulations ($\lambda \lesssim \xi_\parallel$), which are those responsible for the membrane "roughness" and excess area. At zero shear, neighboring membranes collide with one another with mean distance $\xi_\parallel$ between consecutive collisions. These short wavelength undulations interfere with the shear flow. As a result of this coupling, the macroscopic viscosity η_e is increased above the solvent viscosity η_s [28,29]. But at the same time this coupling should also suppress the thermal undulations [21] so as to diminish the macroscopic viscosity and the resulting energy dissipation in the system.

Our focus here will be on low shear rates corresponding to *small Deborah numbers* associated with single membrane undulations $De = \dot\gamma \tau_{\xi_\parallel} \ll 1$ [11], where $\tau_{\xi_\parallel}$ is the undulation relaxation time of a membrane patch of size $\xi_\parallel$, $\tau_{\xi_\parallel} = \eta \xi_\parallel^3/\kappa$ (η is the solvent viscosity and κ is the bending modulus). Hence the flow is only weakly perturbing these short wavelength modes.

Consider a single displacement mode, $h(x) = h_q \sin(qx)$, $q\xi_\parallel \gg 1$. Under steady shear flow, this mode is perturbed (deformed) and the maxima/minima positions are shifted by $\pm\delta x$, see Figure 2. The magnitude of δx is determined from the mechanical equilibrium in the x-direction, *i.e.*, from the balance of the shear force with the membrane elastic forces. In the non-perturbed state, the bending energy (per unit area) is $E_o \simeq \frac{1}{2}\kappa q^4 h_q^2$. For the perturbed state we write $E = E_o + \delta E(\delta x)$. Now, without considering the details of the shear force (which are associated with the shape of sine wave), the shear force is $f_\eta \propto \eta\dot\gamma$. The membrane elastic restoring force is $f_\kappa = -\partial(\delta E)/\partial(\delta x)$. Equating $-f_\kappa = f_\eta$ we find $\delta x = \delta x(\dot\gamma)$ and so $\delta E = \delta E[\delta x(\dot\gamma)]$. This implies that the restoring force for the mode amplitude h_q (per unit area) in the z direction is

$$f_z = -\kappa q^4 h_q - \frac{\partial \delta E}{\partial h_q} \cdot \tag{1}$$

The second term in equation (1) shows the increase of this force relative to the non-perturbed case. (This is analogous to shearing an initially relaxed spring standing parallel to the z-direction). Now we can view the perturbed modes as the eigenstates of an Hamiltonian that includes both the bending energy and the shear force potential. If $\delta E = \frac{1}{2}\delta E_o h_q^2$, and if solvent molecule collisions with the membrane are unaffected by the shear flow, we can give,

by equipartition theorem, an energy $\frac{1}{2}k_{\rm B}T$ for each perturbed state. The mean square amplitude of h_q in such a steady state is then given by

$$\left\langle h_q^2 \right\rangle \simeq \frac{k_{\rm B}T}{\kappa q^4 + \delta E_{\rm o}(\dot\gamma)} \,. \tag{2}$$

The same result is derived from a Langevin equation for $h_q(t)$ which includes the modified force equation (1) and a white noise force whose correlation function is not modified by the flow (by assumption).

2.2 Approximate perturbation calculation

Let us find approximately δx for small perturbations (low $\dot\gamma$). For this we shall assume $\lambda \simeq h_q$ (*i.e.*, $\kappa \simeq k_{\rm B}T$). The shear force per unit area can be estimated in this case to be $f_\eta \simeq q^2\eta\dot\gamma h_q^2$. To find the elastic restoring force, the perturbed mode (Fig. 2) is taken to be roughly composed of half of a sign period of wavelength $\lambda' = \lambda + 4\delta x$, and half of a sign period of wavelength $\lambda'' = \lambda - 4\delta x$, where $\delta x \ll \lambda$ is assumed, $\lambda = 2\pi/q$. Accordingly the energy of the perturbed mode is estimated to be $E = E_{\rm o} + \delta E$ with

$$\delta E \simeq \frac{12}{\pi^2}\kappa q^4 h_q^2 (q\delta x)^2 \tag{3}$$

which leads to $f_\kappa \simeq -\frac{24}{\pi^2}\kappa q^6 h_q^2 \delta x$. Equating $-f_\kappa = f_\eta$ we find

$$\delta x \simeq \frac{\pi^2}{24}\frac{\eta\dot\gamma}{\kappa q^4} \tag{4}$$

and the mean square amplitude under shear is therefore

$$\left\langle h_q^2 \right\rangle \simeq \frac{k_{\rm B}T}{\kappa q^4 + \frac{\pi^2}{24}\frac{\eta^2\dot\gamma^2}{\kappa q^2}} \,. \tag{5}$$

The second term in the denominator in equation (5) is of course assumed small compared to the first ($De \ll 1$).

Equation (5) is essentially the "Maxwell effect" [30] for the single membrane undulations. Indirect experimental evidence for this effect appears in the X-ray diffraction measurements of a lamellar phase under shear carried out by Yamamoto and Tanaka [22]. They observed *broadening* of the lamellar Bragg peaks which may be explained by the reduction of the compression modulus. This implies an increase of collision length $\xi_\parallel$ which signifies the suppression of thermal undulations. It is easy to show from equation (5) that $\xi_\parallel$ is indeed slightly increased by shear, by calculating the new length for which $\langle h^2 \rangle = d^2$. Similar discussions have been presented by Ramaswamy [21] (who considered velocity gradients within the planes) and by Bruinsma and Rabin [11].

2.3 Shear induced pressure/tension

In the absence of boundary walls, the projected area $A_{\rm o}$ is free to adjust and so is the excess area $\Delta A = A - A_{\rm o}$. The excess area is then decreased by shear and the projected area is increased by the same amount, conserving the total membrane area. However, as will be argued later, we should think of a membrane in the lamellar phase has having confining walls which prevent from the projected area to increase. In this case, assuming that at zero shear rate the pressure vanishes, the membrane will exert a pressure on the walls for any $\dot\gamma > 0$. We may compute this pressure by introducing a Lagrange multiplier σ that couples to the area and corresponds to a pressure $\Pi = \sigma$, thereby

$$\left\langle h_q^2 \right\rangle \simeq \frac{k_{\rm B}T}{\kappa q^4 + \frac{\pi^2}{24}\frac{\eta^2\dot\gamma^2}{\kappa q^2} - \sigma q^2} \,. \tag{6}$$

The excess area can be then calculated according to

$$\frac{\Delta A}{A_{\rm o}} \simeq \frac{1}{8\pi^2}\int_{\pi/\xi_\parallel}^{\pi/a} {\rm d}^2 q q^2 \left\langle h_q^2 \right\rangle \tag{7}$$

where $\xi_\parallel \simeq (2\pi^3)^{1/2}\left(\frac{\kappa}{k_{\rm B}T}\right)^{1/2} d$. Demanding that the excess area is not changed under the combination of shear flow and pressure, $\Delta A(\dot\gamma, \sigma) = (\Delta A)_{\rm eq}$, we find

$$\sigma \simeq \frac{\pi^4}{18}\frac{\kappa d^4}{(k_{\rm B}T)^2}\eta^2\dot\gamma^2 \,. \tag{8}$$

The pressure is thus quadratic in shear rate.

An equivalent approach is to consider first the supplement to the projected area $\delta A_{\rm o}$ in the *absence* of boundary walls, using the fact that it is equal to the reduction in excess area. The latter is calculated using equations (5, 7) to be

$$\frac{\delta A_{\rm o}}{A_{\rm o}} = \frac{\pi^4}{72}\frac{\eta^2\dot\gamma^2 d^6}{(k_{\rm B}T)^2} \,. \tag{9}$$

This addition to the projected area can also be thought as resulting from a balance between two opposing forces, in which the membrane is considered initially in equilibrium: an external *tension* (*i.e.*, an outward pressure) due to the shear, which acts to increase the projected area, and a restoring force associated with an increase of the (shear-free) membrane free-energy. The Helmholtz free-energy density (per unit area) for a membrane confined between two parallel walls (in the absence of flow) has been evaluated in reference [11] for small deviations of the area ratio $A/A_{\rm o}$ from the equilibrium one $(A/A_{\rm o})_{\rm eq}$ (see also Appendix A) to be

$$f_{\rm mem} \simeq \frac{3\pi^2(k_{\rm B}T)^2}{128\kappa d^2} + \nu\frac{\kappa}{d^2}\left[\frac{A}{A_{\rm o}} - \left(\frac{A}{A_{\rm o}}\right)_{\rm eq}\right]^2 \tag{10a}$$

where

$$\nu = \frac{9\pi^2}{2(1-4/\pi^2)} \tag{10b}$$

and

$$\left(\frac{A}{A_{\rm o}}\right)_{\rm eq} \simeq 1 + \frac{k_{\rm B}T}{4\pi\kappa}\ln\left[\sqrt{\frac{8}{3}}\left(\frac{\kappa}{k_{\rm B}T}\right)^{1/2}\frac{d}{a}\right] \tag{10c}$$

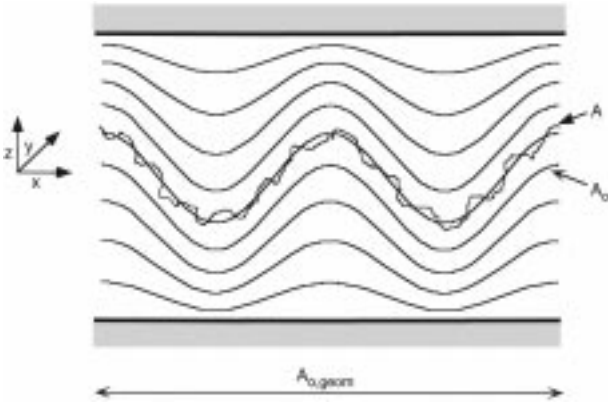

Fig. 3. Undulation instability of a lamellar phase according to equation (22), which describes a stripe modulation in the **x**-axis (the amplitude is exaggerated large). The flow is assumed to be in the **y**-direction, so that it does not deform the structure.

where a denotes the membrane thickness. The first term in equation (10a) is the familiar Helfrich repulsion associated with the entropy cost of confining the membrane. The second term shows that the membrane responds to changes in its projected area like a spring. The free-energy penalty $\delta f_{\rm mem}$ when the projected area $A_{\rm o}$ is perturbed (at constant area A) near its equilibrium value, $A_{\rm o} = A_{\rm o}^{(\rm eq)} + \delta A_{\rm o}$, is then

$$\delta f_{\rm mem} \simeq \nu \frac{\kappa}{d^2} \left(\frac{A}{A_{\rm o}}\right)^2_{\rm eq} \left(\frac{\delta A_{\rm o}}{A_{\rm o}}\right)^2 . \qquad (11)$$

Under external tension $\sigma(\dot\gamma)$ the *Gibbs* free-energy variation is given by $\delta G_{\dot\gamma} = -\sigma \delta A_{\rm o} + A_{\rm o} \delta f_{\rm mem}$. The new projected area is then found by minimizing $\delta G_{\dot\gamma}$ with respect to $\delta A_{\rm o}$. Here we use this procedure to deduce σ making use of equation (9) for $\delta A_{\rm o}$. The result (taking $(A/A_{\rm o})_{\rm eq} \simeq 1$) is

$$\sigma \simeq \frac{\pi^6}{8(1-4/\pi^2)} \frac{\kappa d^4}{(k_{\rm B}T)^2} \eta^2 \dot\gamma^2 . \qquad (12)$$

Note that the difference in the results (12) and (8) is only in the numerical prefactor. While we cannot judge which of the two results is more accurate, consistency with our calculation for buckling of the lamellar phase given below requires that we use equation (12).

3 Lamellar phase elastic response to shear

We have seen that the effect of the shear flow on each individual membrane is to increase (at constant A) the projected area over its zero shear value, so as to decrease the excess area $\Delta A = A - A_{\rm o}$. If there are boundary walls which prevents the increase of projected area, there is a lateral pressure exerted at the walls equation (8). Therefore, under a large enough pressure the whole lamellar phase may buckle coherently (see Fig. 3). This buckling will involve an elastic energy penalty which we will consider in this section. It is similar to the buckling of a plate under compression. A perhaps better analogy is that of a plate – confined by walls at its circumference – which attempts to undergo, say, a longitudinal thermal expansion, which may then lead to its buckling. (The difference between these two analogies is however only semantic; for given final temperature and projected area, the final buckling state is the same no matter which of the two routes is considered).

In order to proceed we distinguish between two type of projected areas (Fig. 3): (i) the *geometric* projected area ($A_{\rm o,geom}$ in Fig. 3), which we define as the projected area associated with membrane wrinkles at *all* length scales (be it thermal undulations, buckling, etc.), and (ii) the *physical* projected area $A_{\rm o}$, which we *define* as the one resulting *only* from the *short wavelength* roughness, $\lambda \lesssim \xi_\parallel$. In the lamellar phase the *geometric projected* area is the one which is (usually) fixed by the physical dimensions of the system, accounted for by our fictitious boundary walls. For example, in a couette cell each membrane has a fixed geometric projected area (*i.e.*, the area of a cylinder) if its mean cylindric radius (the radius from the axis of symmetry of the cell) is not allowed to change. The mean radius may change only by allowing the solvent to permeate through the membranes. However, this relaxation channel will usually be very slow compared to other relaxation channels, so it may be ignored [31]. On the other hand, the *physical* projected area may increase by *buckling*.

It is thus perhaps more appropriate to speak about a shear induced *tension* which couples to the physical projected area (and works to increase it), rather than a pressure which would couple instead to the geometric area (and would work to decrease it). This tension may be also thought of as an effective chemical potential for the projected area. The term "tension" will be therefore used henceforth throughout the paper, even though the reason for using this term, and not a "pressure", is mainly semantic. (This difference is similar to the one between the two analogies of plate buckling given above).

The model of a single membrane "sandwiched" between two parallel walls is a convenient tool to manifest the difference between the two projected areas, physical and geometric. When the walls are flat (and parallel to each other), both projected areas are identical and are simply the area of projection on one of the walls (or on the middle surface). Suppose now that the two walls buckle sinusoidally in a coherent fashion, and that the wavelength of buckling is much greater than $\xi_\parallel$. According to our definitions the area of projection on one of the walls remains the physical projected area. The area of projection onto the planar surface is our geometric projected area. This distinction is possible because of the separation of length-scales between the short wavelength roughness and the long wavelength buckling. We can distinguish similarly between the physical and geometric excess areas.

Consider first a *hypothetical* lamellar domain whose boundaries are free to expand into a pure solvent region. Here the new, steady shear, projected area, is given by equation (9). As discussed above, if the geometric projected area is fixed, the physical projected area has

to *buckle* in order to increase (Fig. 3). The single membrane free-energy cost (Eq. (11)) against the increase of projected area is associated with simple dilatation *parallel* to the membrane mean planes. When the lamellar buckles (on a long wavelength scale, $\lambda \gg \xi_{\parallel}$), there are also Helfrich bending energy and compression energy costs. The first is resulting from the bending of each layer. The second is associated with local changes in the interlayer spacing $d \to d + \delta d$. These produce an energy variation resulting from the first term in equation (10a) (which produces a penalty for negative δd), and also from changing the equilibrium value of the area ratio according to equation (10c), which leads to an energy cost (for both positive and negative δd) resulting from the second term in equation (10a). Using the usual smectic displacement field $U(\mathbf{r})$, we have, according to simple differential geometry,

$$\delta d \simeq d\left(\frac{\partial U}{\partial z} - \frac{1}{2}\left(\nabla_{\perp} U\right)^2\right). \tag{13}$$

This leads to a generalized Landau-de-Gennes free-energy for long wavelength deformations of the lamellar

$$\begin{aligned} F_{\rm lam} = \int \mathrm{d}^3 r \Bigg[& \frac{1}{2} K \left(\nabla_{\perp}^2 U\right)^2 \\ & + \frac{1}{2}\tilde{B}\left(\frac{\partial U}{\partial z} - \frac{1}{2}\left(\nabla_{\perp} U\right)^2\right)^2 + \nu \frac{\kappa}{d^3}\left(\frac{A}{A_{\rm o}}\right)_{\rm eq}^2 \Delta(\mathbf{r})^2 \\ & + \frac{\nu}{2\pi}\frac{k_{\rm B}T}{d^3}\left(\frac{A}{A_{\rm o}}\right)_{\rm eq} \Delta(\mathbf{r})\left(\frac{\partial U}{\partial z} - \frac{1}{2}\left(\nabla_{\perp} U\right)^2\right)\Bigg] \end{aligned} \tag{14a}$$

with

$$\Delta(\mathbf{r}) = \frac{\delta A_{\rm o}}{A_{\rm o}} \tag{14b}$$

denoting the coarse-grained local change in the physical projected area $A_{\rm o}$. In equation (14a), the first term represents the Helfrich cost for bending the layers with bending elastic modulus K, while the second term is the compression energy cost for allowing the interlayer distance to change, with $\tilde{B}$ denoting the compression modulus. These are related to the single layer bending modulus κ and the interlayer distance d by

$$K = \kappa/d \tag{15a}$$

and

$$\tilde{B} = \bar{B} + \frac{\nu}{16\pi^2}\frac{(k_{\rm B}T)^2}{\kappa d^3} = \left(\frac{9\pi^2}{64} + \frac{\nu}{16\pi^2}\right)\frac{(k_{\rm B}T)^2}{\kappa d^3}\,. \tag{15b}$$

The third tern in equation (14a) is identical to equation (11) and represent the cost of stretching or compressing the physical projected area. The last term represents a coupling between local stretching and displacement.

In equation (15b) $\bar{B}$ is the familiar compression modulus at *constant chemical potential* (*c.f.*, Eq. (B.4), Appendix B). Recall that constant chemical potential corresponds to the second term in equation (10a) being a constant (which can thus be omitted). If we would now introduce a variation of the interlayer spacing in the remaining first (Helfrich repulsion) term in equation (10a), this will lead to the familiar free-energy at constant chemical potential equation (B.4), which appears like the first two terms in equation (14a) but with $\bar{B}$ replacing $\tilde{B}$. Likewise, minimizing equation (14a) over $\Delta(\mathbf{r})$ also leads to the same (constant chemical potential) free-energy, equation (B.4).

We note in passing that a more familiar free-energy, that includes the local surfactant (membrane) *concentration* as the extra variable (instead of $\Delta(\mathbf{r})$), can be derived from equation (10) [11,32], see Appendix B. However, equation (14) is a more appropriate starting point for our purposes. First, as argued above, the shear couples directly to the physical projected area (and not to the concentration) through the induced tension. Second, equation (14) allows us to consider free-energy changes at constant membrane area A, which we believe to be the appropriate constraint for our problem (see below).

Given the lamellar elastic free-energy that is opposing a virtual change in the local (physical) projected area, we may construct the total (virtual) *Gibbs*-like free-energy, in which the shear flow is represented by an external tension which couples to the physical projected area (see Sect. 2.3),

$$G_{\dot{\gamma}} = -\frac{\sigma}{d}\int \mathrm{d}^3 r \Delta(\mathbf{r}) + F_{\rm lam}. \tag{16}$$

Note that although equation (16) (with Eq. (14)) is rotationally invariant for arbitrarily large rotations, the term in σ was constructed only for a lamellar which is nearly in "c" orientation (*i.e.*, layer normals orient parallel to the velocity gradient direction), and it does not describe correctly large deviations from this orientation; true rotational invariance is absent for $\dot{\gamma} > 0$ but this is not described by this equation.

The procedure for determining the relation between $\Delta(\mathbf{r})$ and $U(\mathbf{r})$ under shear depends on physical assumptions. It could be argued that equation (16) should be minimized over $\Delta(\mathbf{r})$. If so we obtain

$$\Delta(\mathbf{r}) = -\frac{k_{\rm B}T}{4\pi\kappa}\left(\frac{\partial U}{\partial z} - \frac{1}{2}\left(\nabla_{\perp} U\right)^2\right) + \frac{\sigma d^2}{2\nu\kappa} \tag{17}$$

which leads to

$$\begin{aligned} G_{\rm nc} = \int \mathrm{d}^3 r \Bigg[& -\frac{k_{\rm B}T\sigma}{8\pi\kappa d}\left(\nabla_{\perp} U\right)^2 \\ & + \frac{1}{2}K\left(\nabla_{\perp}^2 U\right)^2 + \frac{1}{2}\bar{B}\left(\frac{\partial U}{\partial z} - \frac{1}{2}\left(\nabla_{\perp} U\right)^2\right)^2\Bigg]. \end{aligned} \tag{18}$$

(We have set $(A/A_{\rm o})_{\rm eq} = 1$ for simplicity and used the boundary conditions $U(0) = U(D) = 0$, which break the rotational invariance.) The first, destabilizing, term in equation (18) can lead to an undulation (buckling) instability – similar in some respect to the one discussed in Section 4 – which originates from the fact that the local

interlayer spacing is forced to follow a smaller excess area according to the equilibrium condition (*cf.*, Eq. (10c)). *However*, this procedure does *not* conserve the *total* membrane area (including the short wavelength roughness) in each layer. We believe that this is not appropriate for the experiments we discuss. For if surfactant exchange between each layer and a "reservoir" (of constant chemical potential) could take place within the experimental timescale (*e.g.*, several minutes), the system would prefer to nucleate another membrane layer – in order to decrease d – rather than to buckle at constant number of layers. Therefore we shall assume henceforth that, in the non-equilibrium transitions we consider, the *total* membrane area in each layer (and the number of layers) *cannot change* during shear, and *we will not use equation (18).* For experiments where membrane area can change (but the number of layers cannot), equation (18) could be a useful starting point. We shall examine the implications of equation (18) briefly in Section 4.4.

Keeping now constant the total membrane area and the geometric projected area in each layer, can be translated to the following constraint on the (total) change in the physical projected area [33]

$$\int \mathrm{d}^2x \Delta(\mathbf{r}) \simeq \int \mathrm{d}^2x \frac{1}{2} \left(\nabla_\perp U(\mathbf{r})\right)^2 . \tag{19}$$

(The integrals in Eq. (19) are over the geometric projected area). For simplicity, we shall avoid here the minimization of $G_{\dot\gamma}$ over $\{\Delta(\mathbf{r})\}$ subject to the constraint equation (19), and instead replace this global constraint by a local one

$$\Delta(\mathbf{r}) \simeq \frac{1}{2} \left(\nabla_\perp U(\mathbf{r})\right)^2 \tag{20}$$

which of course agrees with the global constraint. (This turns out to be a very good approximation to the full minimization; the final results are almost identical in both procedures). We thus obtain $G_{\dot\gamma}$ as a functional of $\{U(\mathbf{r})\}$ alone

$$\begin{aligned} G_{\dot\gamma} = \int \mathrm{d}^3r \Bigg[& -\frac{1}{2}\frac{\sigma}{d} \left(\nabla_\perp U\right)^2 + \frac{1}{2} K \left(\nabla_\perp^2 U\right)^2 \\ & + \frac{1}{2}\tilde{B} \left(\frac{\partial U}{\partial z}\right)^2 + \frac{1}{8} B_\mathrm{e} \left(\nabla_\perp U\right)^4 \\ & - \frac{1}{2} C_\mathrm{u} \frac{\partial U}{\partial z} \left(\nabla_\perp U\right)^2 \Bigg] \end{aligned} \tag{21a}$$

where

$$B_\mathrm{e} \simeq \tilde{B} + 2\nu \frac{\kappa}{d^3} \left(\frac{A}{A_\mathrm{o}}\right)^2_\mathrm{eq} - \frac{\nu}{\pi} \frac{k_\mathrm{B}T}{d^3} \left(\frac{A}{A_\mathrm{o}}\right)_\mathrm{eq} \tag{21b}$$

$$C_\mathrm{u} = \tilde{B} + \frac{\nu}{2\pi} \frac{k_\mathrm{B}T}{d^3} \left(\frac{A}{A_\mathrm{o}}\right)_\mathrm{eq} . \tag{21c}$$

Note that the term proportional to σ is negative, showing that it acts to *increase* the physical projected area (at constant geometric projected area). That a lamellar phase under shear flow is fully described by this effective thermodynamic potential is clearly an assumption, but it has the advantage that the problem is now reduced to a free-energy minimization. Next we apply this model to study the possibility of buckling of a lamellar phase under shear.

4 Buckling instability

4.1 Linear profile analysis

As for the case of a "plate" under compression, we may expect that above a critical value of σ the lamellar phase will buckle. Near this transition (which is yet to be found) we may assume a single mode buckling modulation [13]. Let us first consider a stripe modulation along (say) the x-axis (Fig. 3). This will be compared later to a square lattice modulation. We shall also take only the first harmonic of the z dependent amplitude which should satisfy vanishing boundary conditions at the top and bottom surfaces. Thus

$$U(\mathbf{r}) = U_\mathrm{o} \sin\left(\frac{\pi}{D} z\right) \cos\left(qx\right). \tag{22}$$

Here it is assumed that q is independent of z. This is not entirely correct. In fact, for very small buckling amplitudes where $U_\mathrm{o} \ll d$ each layer may buckle at a slightly different q. However, as soon as $U_\mathrm{o} \sim d$ neighboring layers with different wavelength modulations will cut each other, which is obviously not permissible. Therefore we may expect that the repulsion between layers (*i.e.*, the compression energy) will drive the system to buckle with all layers having the same wavelength. Our purpose is then to find this wavelength self-consistently with the assumption that it is independent of z.

Using equation (22) in equation (21a) and performing the 3-D integration, we obtain the free-energy density $\tilde{g}_{\dot\gamma} = G_{\dot\gamma}/V$ ($V = L_x L_y D$ is the volume) as

$$\tilde{g}_{\dot\gamma} = \frac{1}{8} \left[K q^4 + \tilde{B}\frac{\pi^2}{D^2} - \frac{\sigma}{d} q^2 \right] U_\mathrm{o}^2 + \frac{9}{512} B_\mathrm{e} q^4 U_\mathrm{o}^4 . \tag{23}$$

Note again that the term in σ is negative, even though it couples to $\sim q^2 U_\mathrm{o}^2$. From our standpoint the latter expression simply accounts for the change in the physical projected area.

Buckling occurs when the square brackets in equation (23) first become negative. To find the characteristics of this buckling transition we need to minimize equation (23) over q and U_o. We shall use the complete expression in equation (23), and not only the U_o^2 term, since the coefficient of U_o^4 depends on q and we shall be interested in the preferred value of q also away from the transition. The critical "tension" is found to be

$$\sigma_\mathrm{c} = 2\pi\sqrt{K\tilde{B}}\frac{d}{D} \simeq 8.57 \, \frac{k_\mathrm{B}T}{Dd} . \tag{24}$$

This corresponds to a critical shear rate

$$\dot\gamma_\mathrm{c} \simeq 0.2 \frac{(k_\mathrm{B}T)^{3/2}}{\eta \kappa^{1/2} d^{5/2} D^{1/2}} . \tag{25}$$

The preferred wavenumber is

$$q_{\rm co} = \left(\frac{\pi}{D}\right)^{1/2}\left(\frac{\tilde{B}}{K}\right)^{1/4} \simeq 2.07\,\left(\frac{k_{\rm B}T}{\kappa d D}\right)^{1/2}. \qquad (26)$$

In equations (24, 26) the second equality holds for lamellar phases stabilized by the Helfrich undulation forces, equations (15a, 15b). The reason for a finite $q_{\rm co}$ is the cost of compression energy. Without it (*i.e.*, when $\tilde{B} = 0$) the preferred value of q would have been zero (or π/L_x, the low cutoff). Interestingly, $q_{\rm co}$ becomes exactly the critical wavenumber obtained for the more familiar undulation instability under dilatation in the z-direction [13] (*i.e.*, dilatation perpendicular to the layers), if we replace $\tilde{B}$ by $\bar{B}$. This is not too surprising since the $U_{\rm o}^2$ term in equation (23) becomes identical in this case to the one appearing for dilatation if we also set $\sigma/d = \bar{B}\gamma_z$ where $\gamma_z = \delta D/D$ is the strain. Because of the q^4 dependence of the $U_{\rm o}^4$ term, this wavenumber is found to be the one preferred even away from the transition. This result will be modified when we apply next non-linear analysis.

To complete the linear analysis, the buckling amplitude is found (from minimization over $U_{\rm o}$) to obey the relation

$$U_{\rm o} q_{\rm co} = \frac{4\sqrt{2}}{3}\sqrt{\frac{\sigma-\sigma_{\rm c}}{B_{\rm e} d}}\,. \qquad (27)$$

Note that $U_{\rm o} \sim \sqrt{\sigma-\sigma_{\rm c}}$, as expected for a "mean-field" type model.

4.2 Non-linear profile analysis

While in the previous section we attempted to analyze the undulation instability even away from the threshold (by including the $U_{\rm o}^4$ term), the sine profile considered is accurate only in the critical sense, and the use of such an ansatz for non-critical systems is not justified. We thus consider now the undulation instability far from criticality in a more consistent way [20]. We focus on the z-dependent amplitude and its deviation from a pure sine function; we are not concerned here about the evolution of the geometrical structure itself beyond the single harmonic modulation. Instead of equation (22) we thus use

$$U(\mathbf{r}) = u(z)\cos\,(qx) \qquad (28)$$

where $u(z)$ will be found by free-energy minimization. Substituting into equation (21a) we obtain

$$g_{\dot\gamma} \equiv \frac{G_{\dot\gamma}}{L_x L_y} = \int_0^D {\rm d}z\left[-\frac{1}{2}au(z)^2 + \frac{1}{4}bu(z)^4 + \frac{1}{4}\tilde{B}\left(\frac{\partial u}{\partial z}\right)^2\right] \qquad (29a)$$

where we have set

$$a(q) = \frac{1}{2}\left(\frac{\sigma}{d}q^2 - Kq^4\right) \qquad (29b)$$

and

$$b(q) = \frac{3}{16}B_{\rm e}q^4. \qquad (29c)$$

Equation (29a) resembles the familiar 1-D Landau-Ginzburg free-energy, and we may use the available knowledge for this well studied model. First, we note that for the pure bulk behavior we may set $\partial u/\partial z = 0$ and equation (29a) becomes the usual Landau free-energy. Its minimum is obtained for $u = \sqrt{a/b}$. We may therefore expect that for very large D, or for σ much above the threshold, equation (29a) with $\partial u/\partial z = 0$ will describe most of the interior of the slab. To understand how the amplitude decays to zero on approaching the walls, we first recall the case of a semi-infinite bulk region ($z \geq 0$). The Euler-Lagrange equations corresponding to equation (29a) are

$$\frac{1}{2}\tilde{B}\frac{\partial^2}{\partial z^2}u = -au + bu^3 \qquad (30)$$

with the boundary conditions $u(0) = 0$ (due to the presence of a flat wall) and $\partial u/\partial z|_{z\to\infty} = 0$. (Note that if the u^3 term is neglected, the solution to this differential equation for our slab problem $u(0) = u(D) = 0$ is a pure sine, consistent with equation (22).) To solve equation (30), we multiply it by u and integrate once to obtain

$$\frac{1}{4}\tilde{B}\left(\frac{\partial u}{\partial z}\right)^2 = -\frac{1}{2}au(z)^2 + \frac{1}{4}bu(z)^4 + \frac{a^2}{4b} \qquad (31)$$

where the constant of integration $a^2/4b$ was found by using the boundary conditions $\partial u/\partial z|_{z\to\infty} = 0$ and $u(\infty) = \sqrt{a/b}$. This allows us to write the right hand side of equation (31) as a complete square $\frac{1}{4}b\left(u^2 - a/b\right)^2$, which in turn enables to integrate a second time to give

$$u(z) = \sqrt{\frac{a}{b}}\tanh\left(\frac{z}{\xi}\right). \qquad (32a)$$

Here we have defined the correlation length

$$\xi = \sqrt{\frac{\tilde{B}}{a}}\,. \qquad (32b)$$

Equation (32) is a well known result for this boundary value problem [3,1]. It allows us to quantify the criterion for validity of the linear stability discussed in Section 2. If $\xi \gtrsim D$ the linear analysis is accurate; it breaks down when $\xi \ll D$. As can be seen ξ diverges at the (bulk) buckling transition ($a \to 0$). At finite gap conditions its critical value is $\xi = D/\pi$, which means that the linear analysis should be accurate close to the transition, as expected. Equation (32) should be reasonably accurate, on the other hand, when $D \gg \xi$, for z in the range $0 < z < D/2$. (For z in the range $D/2 < z < D$ the result is obtained by replacing z by $D - z$.)

Let us estimate ξ when σ is not critical but still on the order of $\sigma_{\rm c}$. Than $a \sim \sigma_{\rm c}q_{\rm c}^2/d \sim (k_{\rm B}T)^2/(\kappa d^3 D^2)$ so that $\xi \sim D$. Hence the sine, linear analysis, form, for $u(z)$,

introduced in equation (22), should be marginally correct even outside true criticality. However, we now want to find more accurately how the preferred wavenumber q_c evolves away from its critical value q_{co} when σ is varied away from the transition, $\sigma > \sigma_c$. Note that the value of q that minimizes the bulk free-energy (Eq. (29) with $\partial u/\partial z = 0$) is vanishing, *i.e.*, q_c obtains its low cutoff value π/L_x, and so does the critical tension, $\sigma_c \sim \kappa/L_x^2$. Yet, buckling cannot not occur at such small tensions since this is not self-consistent with the assumption $\xi \ll D$. Rather we have $\xi \sim L_x^2/d \gg D$, which implies that q_c obtains a different value.

The method described below, which is commonly used in Landau-Ginzburg type boundary value problems (*e.g.*, for polymer adsorption on surfaces), allows us to find q_c without reference to a particular (non-harmonic) shape of the amplitude profile $u(z)$. Let us denote by U_o the value of $u(z)$ at the middle plane, $z = D/2$, which is therefore also the maximum value that $u(z)$ obtains in the whole slab. From the requirements of (i) symmetry of $u(z)$ around the middle plane and (ii) analyticity of $u(z)$ at the middle plane, we must have $\partial u/\partial z|_{D/2} = 0$. Equation (31) is then replaced by

$$\frac{1}{4}\tilde{B}\left(\frac{\partial u}{\partial z}\right)^2 = -\frac{1}{2}a\left(u(z)^2 - U_o^2\right) + \frac{1}{4}b\left(u(z)^4 - U_o^4\right). \quad (33)$$

Using this relation to eliminate $\partial u/\partial z$ in equation (29) we obtain

$$g_{\dot\gamma} = \left(\frac{1}{2}aU_o^2 - \frac{1}{4}bU_o^4\right)D + \int_0^D \mathrm{d}z\left[-au(z)^2 + \frac{1}{2}bu(z)^4\right]. \quad (34)$$

Transforming the integral over z to an integral over u, using again equation (33), we obtain, after some manipulations, a general integral expression for the free energy

$$g_{\dot\gamma} = \left(\frac{1}{2}aU_o^2 - \frac{1}{4}bU_o^4\right)D + 2\sqrt{\frac{\tilde{B}}{b}}\int_0^{U_o}\mathrm{d}u\frac{-au^2 + \frac{1}{2}bu^4}{\sqrt{(2a/b - U_o^2 - u^2)(U_o^2 - u^2)}}. \quad (35)$$

The "constant of integration" U_o is determined *uniquely* from the following identity

$$D = 2\int_0^{D/2}\mathrm{d}z = 2\sqrt{\frac{\tilde{B}}{b}}\int_0^{U_o}\frac{\mathrm{d}u}{\sqrt{(2a/b - U_o^2 - u^2)(U_o^2 - u^2)}} \quad (36)$$

(in contrast to the direct minimization over U_o in the linear analysis). The integrals in equations (35, 36) can be expressed in terms of known elliptic integral functions [20]; see Appendix C. However, they cannot be calculated analytically. We shall therefore obtain explicit results only for two regimes: (i) $\xi \sim D$ which will correspond to $\sigma \sim \sigma_c$ and (ii) $\xi \ll D$ which will correspond to $\sigma \gg \sigma_c$.

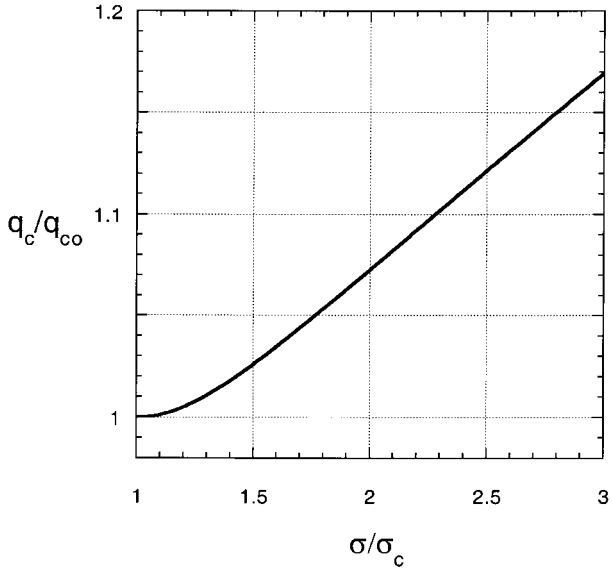

Fig. 4. Preferred wavenumber q_c, reduced by its value q_{co} at $\sigma = \sigma_c$, against the reduced tension σ/σ_c.

Consider first $\xi \sim D$. Here we expect $U_o \ll \sqrt{a/b}$. Expanding the integrands in equations (35, 36) appropriately we obtain

$$g_{\dot\gamma} \simeq \left(\frac{1}{2}Da - \frac{\pi}{2\sqrt{2}}\sqrt{\tilde{B}a}\right)U_o^2 - \left(\frac{1}{4}Db + \frac{\pi}{32\sqrt{2}}\sqrt{\frac{\tilde{B}}{a}}b\right)U_o^4 + o(U_o^6) \quad (37)$$

and

$$\sqrt{\frac{2a}{\tilde{B}}}\frac{D}{\pi} \simeq 1 + \frac{3b}{8a}U_o^2 + o(U_o^4). \quad (38)$$

We may thus eliminate U_o from equation (37) using equation (38). In order to remain within the $o(U_o^6)$ expansion, we first substitute D as a function of U_o in equation (37) and keep terms only up to U_o^4 (The term in U_o^2 is found to cancel out identically). We then substitute back U_o as a function of D. This leads to

$$g_{\dot\gamma}(q) \simeq -\frac{\sqrt{2}\pi}{3}\sqrt{\tilde{B}}\frac{a^{3/2}}{b}\left(\sqrt{\frac{2a}{\tilde{B}}}\frac{D}{\pi} - 1\right)^2. \quad (39)$$

Note that $g_{\dot\gamma}$ depends on q through $a(q)$ and $b(q)$, and may be written as a function solely of q/q_{co} and σ/σ_c.

As the last step we now minimize this free-energy over q (to obtain the preferred value q_c), subject to the constraint $U_o^2 > 0$ (*i.e.*, the brackets in Eq. (39) have to be positive). When $\sigma - \sigma_c \ll \sigma_c$, this free-energy is minimum exactly at $q = q_{co}$, equation (26). However, when σ increases we find that q_c increases too. This should be contrasted with our linear stability result where q_{co} remains the preferred q for any σ. It turns out to be too

difficult to obtain the exact analytic dependence of q_c on σ [34]. However, from equation (39) we find that q_c/q_{co} is a function solely of σ/σ_c. In Figure 4 we plot this function which is found numerically using, instead of equation (39), a more accurate free-energy which includes terms up to order U_o^6. It is seen that when $\sigma \sim \sigma_c$, q_c is weakly dependent on σ: q_c/q_{co} increases almost linearly with σ/σ_c with a very small slope, roughly 0.1. For $\sigma \gg \sigma_c$ (not shown in Fig. 4), q_c – determined from equation (39) – becomes much larger than q_{co} and approaches asymptotically the value $(\sigma/6Kd)^{1/2}$. However, using the latter value in equation (32b) we find that $D/\xi \sim \sigma/\sigma_c \gg 1$ which means that the small U_o approximation *entirely breaks down* in this limit. Therefore, we conclude that in the regime of σ where this approximation is valid, *i.e.* $\sigma \sim \sigma_c$, q_c remains roughly equal the critical value q_{co}, equation (26).

Next we consider the regime $\sigma \gg \sigma_c$ which should correspond to $D \gg \xi$. Here $u(z)$ is expected to be roughly constant inside the slab $\xi \ll z \ll D - \xi$, with $u(z) \simeq U_o \simeq \sqrt{a/b}$, the bulk value. Using this value of U_o for the integrands in equations (35, 36) (but not for the upper integration limit) we obtain in this limit

$$g_{\bar{\gamma}} \simeq \left(\frac{1}{2}aU_o^2 - \frac{1}{4}bU_o^4\right) D + \sqrt{\frac{\tilde{B}}{b}}\left(aU_o - \frac{1}{3}bU_o^3 - \frac{a^{3/2}}{\sqrt{b}}\text{arctanh}\left(\sqrt{\frac{b}{a}}U_o\right)\right) \quad (40)$$

and

$$D \simeq 2\sqrt{\frac{\tilde{B}}{a}}\text{arctanh}\left(\sqrt{\frac{b}{a}}U_o\right). \quad (41)$$

Equation (41) shows that indeed $U_o \to \sqrt{a/b}$ as $D \to \infty$, as required. Using it to eliminate the "diverging" inverse hyperbolic tangent from equation (40), and replacing the remaining U_o by $\sqrt{a/b}$ we find

$$g_{\bar{\gamma}} \simeq -\frac{a^2}{4b}D + \frac{2}{3}\frac{\sqrt{\tilde{B}}a^{3/2}}{b} = -\frac{a^2}{4b}\left(D - \frac{8}{3}\xi\right). \quad (42)$$

(An equivalent derivation of Eq. (42) using elliptic integral expansions is presented in Appendix C). The second equality in equation (42) shows that $g_{\bar{\gamma}}$ is simply the bulk free-energy of a slab with an effective reduced size $D - \frac{8}{3}\xi$. This is because the direct contribution from the regions near the walls scales as $\frac{a^2}{b}\xi$. This can be seen from equation (29) by estimating $\frac{\partial u}{\partial z} \sim U_o/\xi$. Note that even though $D \gg \xi$ has been assumed, the linear term in ξ cannot be neglected since, as discussed above, *without it the minimum is at* $q = 0$ (or at $q = \pi/L_x$, the low cutoff), which contradicts the assumption $D \gg \xi$. Minimizing now with respect to q we obtain, within the self-consistent approximation that $\sigma/d \gg Kq^2$ (consistent with the system being far from criticality),

$$q_c \simeq \frac{\sqrt{2}}{3^{\frac{1}{3}}}\frac{(\tilde{B}\sigma)^{1/6}}{d^{1/6}(KD)^{1/3}}. \quad (43)$$

Equation (43) shows that when $\sigma \gg \sigma_c$, q_c is substantially increased from its critical value q_{co}. As required for consistency, in this limit we find $\xi \ll D$. Interestingly, equation (43) coincides – to within a numerical prefactor – with the expression for q_{co} in the limit $\sigma = \sigma_c$. Together with our results for the regime $\sigma \sim \sigma_c$, this suggests that q_c may be described by a single scaling function of the argument σ/σ_c in the whole σ regime, *i.e.* $q_c = q_{co}f(\sigma/\sigma_c)$, where $f(1) = 1$ and $f(x) \sim x^{1/6}$ for $x \gg 1$.

To end this analysis we calculate the amplitude U_o for $\sigma \gg \sigma_c$. Using $U_o = \sqrt{a/b}$ and $\sigma q_c^2/d \gg Kq_c^2$ we immediately obtain

$$U_o q_c \simeq \sqrt{\frac{8\sigma}{3dB_e}} \quad (44)$$

showing that $U_o q_c \sim \sigma^{1/2}$. This result is in fact very similar to the linear analysis result equation (27), except that here we have to use equation (43) for q_c.

4.3 Square-lattice buckling

Let us now compare the free-energy of the stripe, 1-D, buckling assumed so far to that of a 2-D, square lattice, array. Thus we now use in equation (21a)

$$U(\mathbf{r}) = u(z)\cos(qx)\cos(qy). \quad (45)$$

After integration over x and y we obtain a free-energy similar to equation (29a) with $\frac{1}{4}\tilde{B}$ replaced by $\frac{1}{8}\tilde{B}$ and with

$$a(q) = \frac{1}{2}\left(\frac{\sigma}{d}q^2 - 2Kq^4\right) \quad (46a)$$

and

$$b(q) = \frac{5}{32}B_e q^4. \quad (46b)$$

Using $u(z) = \sin(\pi z/D)$ we find that the critical tension σ_c is *identical* to that of a stripe buckling equation (24) and the critical wavenumber is *smaller* than that of a stripe buckling, equation (26), by a factor of $1/\sqrt{2}$,

$$q_{co} = \left(\frac{\pi}{2D}\right)^{1/2}\left(\frac{\tilde{B}}{K}\right)^{1/4}. \quad (47)$$

Comparing $b(q_{co})$ for the two type of lattices, we find that it is smaller for a square lattice. As a result, the free-energy of the square lattice buckling is smaller than that of the stripe buckling. This suggests that if we can neglect the coupling of the buckling modulation itself with the flow, a square lattice buckling is preferred. (A more elaborate consideration is given in Sect. 5).

Considering the other major predictions discussed above for the stripe buckling, we find the following results for the square lattice buckling: (i) For $\sigma \sim \sigma_c$ we have $q \simeq q_{co}$ equation (47), and U_o obeys an equation similar to equation (27) with a prefactor $8/\sqrt{15}$ replacing $4\sqrt{2}/3$. (ii) For $\sigma \gg \sigma_c$, q_c obeys an equation similar to equation (43) with a prefactor $1/3^{\frac{1}{3}}$ replacing $\sqrt{2}/3^{\frac{1}{3}}$, and U_o obeys an equation similar to equation (44) with 16/5 replacing 8/3 in the square root.

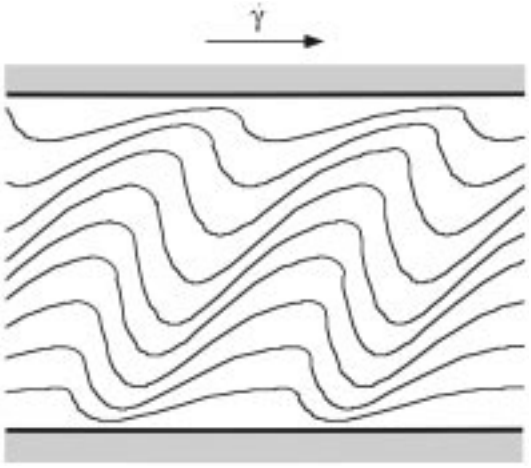

Fig. 5. Deformation of the buckling structure by the flow (schematic illustration). When the deformation is too strong the structure may breakup into onions (Fig. 6).

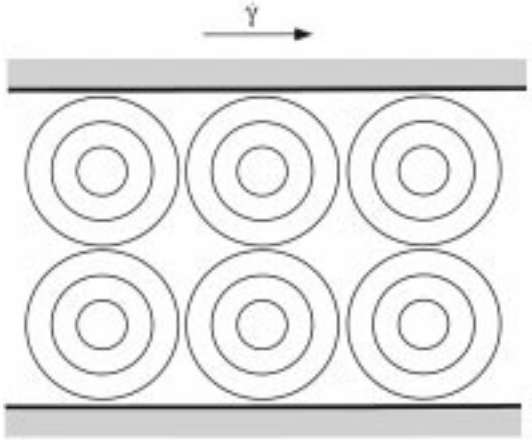

Fig. 6. Formation of onions (schematic illustration). Note that the small number of onions and number of layers (in each onion) is not realistic.

4.4 Non-conserved membrane area

If the system is held at a constant chemical potential, we need not conserve the total membrane material in each layer. If we further assume that due to kinetic reasons the total number of layers cannot change – even though a constant chemical potential does allow such a change – minimization over the local excess area $\Delta(\mathbf{r})$ leads to the free-energy equation (18). The undulation instability resulting from equation (18) is very similar to that found above, even though its physical origin is quite different. Whereas the undulation instability discussed previously is equivalent to the case of a plate under compression, in this case it is equivalent to a dilative strain in the z-direction. The tension σ works to reduce the excess area, and smaller excess area implies that, in an equilibrium-like situation, the interlayer spacing be smaller. If the gap is fixed, this becomes equivalent to a dilative strain.

The results for this case can be obtained simply by making the following replacements in all of the previous results

$$\sigma \to \frac{k_{\mathrm{B}}T}{4\pi\kappa}\sigma \tag{48a}$$

$$\tilde{B} \to \bar{B} \tag{48b}$$

$$B_{\mathrm{e}} \to \bar{B}. \tag{48c}$$

The main effect of these changes is to increase the critical tension (and thus the critical shear rate) of equation (24) by a factor of $4\pi\kappa/k_{\mathrm{B}}T$, which is usually of order 10. As we discussed in Section 2, for shear experiments in a couette cell [10] we believe that this discussion is not relevant; however, it may be appropriate for other cases.

5 Transition to onions

As a last step we wish to connect our results with the observed transition to spherulites, assuming that a square lattice buckling has been selected. We can expect that at some critical shear rate $\dot{\gamma}^*$ the buckling structure will not be stable any longer because of its resistance to the shear flow (Fig. 5). Inspired by the experiments, we shall assume that at this limit of stability the lamellar breaks up into onions (Fig. 6), which can more easily flow by the well known rolling mechanism. These onions should then have an initial size close to the buckling wavelength $\lambda_{\mathrm{c}}(\dot{\gamma}^*)$ (in fact, $\lambda_{\mathrm{c}}/2$).

We now make a concrete estimate for the transition to onions. First we generalize the argument that was used by Roux and co-workers to estimate the onion size, to find the limit of stability of the buckling state. The shear force that a buckling period experience under the flow is $\sim \eta_{\mathrm{e}}\dot{\gamma}U_{\mathrm{o}}\lambda_{\mathrm{c}}$. The elastic lamellar force which opposes this shear force is $\sim \kappa/d$. Balancing the two forces determines *the critical rate for onion formation*. An equivalent estimate, which leads to the *same* scaling result, follows from a closely related discussion of Bruinsma and Rabin [11]. As a result of the shear flow the buckling structure is deformed, see Figure 5. The relaxation time of this deformation is just the familiar undulation mode relaxation time [35]

$$\tau_{\mathrm{q}}^{-1} = \frac{\kappa}{4\eta d}q_{\mathrm{c}}^2. \tag{49}$$

The buckling shape may be destroyed and (presumably) transformed to onions if (say) the maxima are displaced (by this deformation) to the same lateral (say x) position of the neighboring minima. This occurs on a time scale

$$\tau(\dot{\gamma}) = \frac{\lambda_{\mathrm{c}}}{4U_{\mathrm{o}}\dot{\gamma}}\,. \tag{50}$$

Equating the two times we obtain an equation for the critical shear rate for onion formation

$$\dot{\gamma}^* \simeq \frac{\pi}{8}\frac{\kappa q_{\mathrm{c}}^2}{\eta d}(U_{\mathrm{o}}q_{\mathrm{c}})^{-1} \tag{51}$$

where $U = U_{\mathrm{o}}(\dot{\gamma}^*)$ and $q_{\mathrm{c}} = q_{\mathrm{c}}(\dot{\gamma}^*)$. For $\dot{\gamma} > \dot{\gamma}^*$, the deformation does not have time to relax and onions are created (Fig. 6).

To obtain an explicit result, we have to solve equation (51) using the expressions obtained in the previous section for q_c and U_o as a function of the shear rate (effective tension σ). We will first use the (square lattice) results for $\sigma \gtrsim \sigma_c$ (but far from criticality). This will give a lower bound for $\dot{\gamma}^*$. We thus use in equation (51) $q_c \simeq q_{co}$, equation (47), and $U_o q_{co} \simeq \frac{8}{\sqrt{15}}\sqrt{\sigma/B_e d}$. Using also equations (15a, 15b) and (21b) for K, $\tilde{B}$, and B_e, we obtain the "lower bound"

$$\dot{\gamma}_1^* \simeq C_1[k_B T/\kappa]\frac{k_B T}{\eta d^{5/2} D^{1/2}} \tag{52a}$$

where

$$C_1(X) \simeq 0.59\ \left(1 + 0.17\ X + 0.014\ X^2\right)^{1/4} \tag{52b}$$

(*e.g.*, $C_1(1) \simeq 0.62$). Using our (square lattice) results for $\sigma \gg \sigma_c$, namely $q_c \simeq (\tilde{B}\sigma)^{1/6}/3^{1/3} d^{1/6}(KD)^{1/3}$ and $U_o q_c \simeq \sqrt{16\sigma/5dB_e}$, we obtain an "upper bound" for $\dot{\gamma}^*$

$$\dot{\gamma}_2^* \simeq C_2[k_B T/\kappa]\frac{k_B T}{\eta d^{5/2} D^{1/2}} \tag{53a}$$

where

$$C_2(X) \simeq 0.73\ X^{-1/4}\ \left(1 + 0.17\ X + 0.014\ X^2\right)^{3/8} \tag{53b}$$

(*e.g.*, $C_2(1) \simeq 0.78$).

The actual rate is predicted to lie in the interval $\dot{\gamma}_1^* < \dot{\gamma}^* < \dot{\gamma}_2^*$, and its precise value can be found by a numerical solution. It should be noted however that due to the large uncertainty in the numerical factor in equation (51), this remains an academic exercise. Moreover, for $\kappa = k_B T$, $\dot{\gamma}_1^*$ and $\dot{\gamma}_2^*$ are only within 20% of each other and we may therefore conclude that $\dot{\gamma}^* \simeq 0.7\ k_B T/\eta d^{5/2} D^{1/2}$. Note that this has just the *same scaling* form as for $\dot{\gamma}_c$, equation (25), and that $\dot{\gamma}^*$ is only about three-four times greater than $\dot{\gamma}_c$. The buckling state therefore exists in a rather narrow regime of shear rates. The predicted onion size at the transition, which we conjecture to be roughly $\lambda_c(\dot{\gamma}^*)$, is thus close to $\lambda_{co} = 2\pi/q_{co}$, equation (26).

Let us now compare our predictions with the experimental results of Roux and co-workers. We focus on the oil-rich (dodecane) system SDS/pentanol/dodecane/water, with membrane volume fraction $\phi \simeq 0.30$, studied experimentally in reference [16]. For this system $D \simeq 1$ mm, $d \simeq 100$ A, $\eta \simeq 3$ mPa s (the dodecane viscosity), and $\kappa \simeq k_B T$. Using these parameters we get $\dot{\gamma}_c \simeq 10^3$ Hz for the buckling transition critical shear rate and $\dot{\gamma}^* \simeq 3 \times 10^3$ Hz for the transition to onions. This is roughly *three orders of magnitude* above the observed critical rate for onion formation, $\dot{\gamma}^* \sim 1$ Hz. On the other hand, the effective exponent ζ in $\dot{\gamma}^* \sim d^{-\zeta}$ can be estimated from the experimental data [17] to be $\zeta = 2.6 \pm 0.5$, which is *in good agreement* with the theoretical prediction $\zeta = 2.5$. (Of course, because of the apparently large experimental error we cannot exclude the possibility that this agreement is spurious.) The predicted onion size at the transition is ~ 10 μm, which is also roughly *consistent* with the observed onion size.

Yet, how can we understand the huge deviation between the predicted and experimental values for $\dot{\gamma}^*$? A hint for the answer may be given by the very large measured viscosity of the lamellar phase (prior to the transition to onions) $\eta_e \simeq 10^3$ mPa s, which is $\sim 10^3$ times the solvent (dodecane) viscosity. As suggested by Roux and co-workers, this is probably due to the presence of many defects, *e.g.*, dislocations. These defects resist the shear flow and the shear rate must therefore locally vanish inside the defect "cores". Since there is a macroscopic shear rate imposed on the system, local shear rates outside the defects are larger than the imposed shear rate, which should give rise to a larger effective viscosity. Some of these local shear rates may be just as large as the predicted $\dot{\gamma}^*$ so as to induce the transition to onions. While we will not really check this hypothesis here, it seems reasonable to take such effects into account by using in equations (25, 52, 53) the measured viscosity $\eta_e \simeq 10^3$ mPa s, rather than the solvent viscosity $\eta \simeq 3$ mPa s. This ansatz leads to the estimate $\dot{\gamma}^* \simeq 3$ Hz, which is now comparable with the experimental value $\dot{\gamma}^* \sim 1$ Hz. It remains to explore more carefully the role of defects in this phenomena. It might also be useful to use different samples, with different annealing degree, so that the measured viscosity will vary from one sample to the other. If the ansatz is good, one should find $\dot{\gamma}^* \sim 1/\eta_e$.

6 Discussion

As discussed in Section 1, in our free-energy analysis we have neglected the thermal fluctuations of the long wavelength modes and ignored their interaction with the flow. This has been taken into account in the elaborate study of Bruinsma and Rabin [11] (which however did not consider the effect we discuss). Thus the effects of shear flow discussed by Bruinsma and Rabin are not predicted by the present theory. In addition, including the thermal fluctuations of these modes, within a Brazovskii-Fredrickson-Cates type theory [5,6], is expected to change the buckling transition from being second order to (weakly) first order, as well as to somewhat increase the critical shear rate (tension) for the transition. Furthermore, even though the free-energy analysis suggests that buckling to a square lattice is preferred over a stripe lattice, the coupling of these long wavelength unstable modes with the flow may actually prefer a stripe buckling in which the stripes are parallel to the flow. In the latter situation the buckling does not obstruct the flow, unlike for the square-lattice buckling. However, the flow of this type of stripe buckling does involve substantial shearing of the 2-D membrane surface. The two situations can therefore occur in principle, as well as the case of a stripe buckling in which the stripes are perpendicular to the flow. Predicting which one of these three types of buckling will actually be selected must include the 2-dimensional flow of surfactant in the bilayers, which is beyond the scope of this work.

We have conjectured that a buckled lamellar which is deformed to the extent that neighboring minimum and maximum are "sitting" one on top of the other, should

breakup into onions. We may expect however that a lamellar with "stronger" membranes will require a larger deformation than a lamellar with "weak" membranes. We may also expect that a highly buckled lamellar, that does not break into onions, will have a much larger macroscopic viscosity, because of the difficulty of the buckled state to flow. Therefore, if onions are not formed at $\dot{\gamma} = \dot{\gamma}^*$ as discussed above, we may expect a *sharp rise* in stress (or in effective viscosity) for a *small* rise of shear rate, resulting from a corresponding (small) rise of the product $U_o q$. The transition to onions will eventually occur at a higher shear rate. These ideas may explain some of the anomalous stress *vs.* shear rate plots in which an apparent jump in stress appears around the transition to onions [16]. We suggest that this jump may still correspond to a buckled lamellar (and does not signify a transition to onions), and that the actual transition to onions corresponds to the subsequent observed decrease of the effective viscosity. (This is quite different from the explanation given by Roux *et al.* [16].) We are not able at this stage to be more quantitative.

In obtaining our estimate for $\dot{\gamma}^*$ we have used the value of the amplitude in the middle of the gap (*i.e.* at $z = D/2$). This is not entirely accurate since the rest of the system has a smaller amplitude. In fact, what is required to generate just a single layer of onions (centered around $z = D/2$) is that in a whole slab of width λ_c the amplitude becomes larger than the critical one required for formation of onions. This means that U_o (*i.e.* the amplitude at the middle plane) has to be slightly larger than the estimate given in equation (51). It is easy to see however that if (say) the transition occurs at $\dot{\gamma}^* \sim \dot{\gamma}_c$ (where sine amplitude profile applies), this modification only weakly perturb the result for $\dot{\gamma}^*$ since $\lambda_c \ll D$. If $\dot{\gamma}^* \gg \dot{\gamma}_c$, most of the system will generate onions except the narrow slabs of size ξ near the walls where the amplitude falls down rapidly. In an intermediate situation (as discussed in Sect. 4), a slab of some width between λ_c and $D - 2\xi$, centered at the middle, can produce the first generation of onions. Complete transformation of the whole lamellar into an onion state requires that the onion production is followed by repeated phase separation of the onions from the remaining lamellar phase.

7 Conclusions

In this paper we have shown that a lyotropic lamellar phase is unstable against buckling at relatively low shear rates. The instability is related to the coupling of the short wavelength, single membrane, undulations, to the shear flow. While this coupling is weak at the low shear rates considered, the small suppression of these undulations by the flow is enough to produce an increase of the membrane projected area, which latter is forced to buckle in a confined geometry.

An ansatz criterion has been used to determine the buckling amplitude required for the breakup of the buckling texture into an array of onions. When this ansatz is combined with our analytical results for the buckling amplitude and wavelength, we find satisfying agreement with available experimental data provided that we use the experimentally measured viscosity instead of the solvent viscosity.

A non-trivial prediction resulting from the theory is that the critical shear rate for the formation of onions is inversely proportional to the square-root of the gap between the two sliding walls, $\dot{\gamma}^* \sim 1/\sqrt{D}$. The larger this gap is, the lower is the critical shear rate. At the same time, the larger the gap, the larger are the onions generated near the transition. These predictions are yet to be verified in experiment. They can be very important for applications, *e.g.*, for mass production of the onions.

Our theory fails to fully account for the existence of defects. The role of defects may be more important than the one envisaged by the present work, which has been only to increase local shear rates (and, as a result, the effective lamellar viscosity). However, we do predict an undulation instability and formation of onions even in the absence of defects, only that these transitions will occur at higher (imposed) shear rates. This prediction can be checked by annealing (at least partially) any defects existing in the system before commencing the shear.

Our theory is different from most other existing approaches for complex fluids under shear in that it considers a non-equilibrium instability. It is specific to dilute lamellar phases. This suggests, on one hand, that it should be hard to generalize the approach to other systems. On the other hand, the theory shows how internal degrees of freedom of the constituents, even when these only weakly interact with the flow field, can make the whole system become unstable because of their coupling to some other degrees of freedom that are subject to some global constraints. This principle may be occurring in other systems as well.

This research was supported in part by the Israel Science Foundation administered by the Israel Academy of Sciences and Humanities, by the Ministry OF Science and The Arts, Israel, and the French Ministry of Research and Technology, and by The G.M.J. Schmidt Minerva Center for Supramolecular Architectures. We thank Frederic Nallet, Didier Roux, Maurice Kleman, Mike Cates and Robijn Bruinsma for valuable discussions.

Appendix A: Thermodynamics of a single membrane confined between two walls

Here we derive the Helmholtz free-energy of single membrane confined between two walls separated by a gap d. This is used to model a membrane in a lamellar stack. Equivalent derivations can be found in references [11,32,36], but we rederive the main results here in order to put them in the context of the present work.

We start by calculating the grand-canonical potential

$$\Omega = -k_B T \ln \Xi = -k_B T \ln \int \frac{Dh(x)}{\Lambda} \exp[-H(\{h(x)\})/k_B T] \tag{A.1}$$

where Λ is a phase space measure. The Hamiltonian is assumed to be

$$H = \frac{1}{2}\kappa \int_{A_o} \mathrm{d}^2x (\nabla^2 h(\mathbf{x}))^2 + \mu \int_{A_o} \mathrm{d}^2x \left(1 + \frac{1}{2}(\nabla h(\mathbf{x}))^2\right) + \gamma \int_{A_o} \mathrm{d}^2x h^2(\mathbf{x}). \quad (A.2)$$

Here κ is the bending modulus, μ is the surface tension (or chemical potential) Lagrange multiplier of the membrane which couples to the total area A (*i.e.*, to the total number of molecules), γ is the Helfrich Lagrange multiplier which is coupled to the mean square undulation amplitude $\langle h^2 \rangle$, and A_o is the projected area. The two Lagrange multipliers will be determined from the constraints $\partial\Omega/\partial\sigma = \langle A \rangle = A$ and $\partial\Omega/\partial\gamma = A_o\langle h^2 \rangle = A_o \alpha d^2$; here α is a numerical constant which must be smaller than $1/4$ since the maximum value of h is $d/2$. Following Bruinsma and Rabin, it will be determined by consistency with the more accurate calculation of Helfrich of the undulation interaction potential. Transforming to Fourier space, the partition function may be expressed as

$$\Omega = -k_B T \ln \int \prod_{\mathbf{q}} \frac{\mathrm{d}h_{\mathbf{q}} \mathrm{d}h_{-\mathbf{q}}}{a^6} \mathrm{e}^{\frac{\mu A_o}{k_B T}} \times \exp\left[-\frac{1}{2k_B T A_o} \sum_{\mathbf{q}} \left(\kappa q^4 + \mu q^2 + 2\gamma\right) h_{\mathbf{q}} h_{-\mathbf{q}}\right]. \quad (A.3)$$

Performing the integrations, we find for the free-energy density $\omega = \Omega/A_o$

$$\omega = \mu + \frac{k_B T}{8\pi^2} \int \mathrm{d}^2 q \ln\left[\frac{a^6}{2A_o k_B T}\left(\kappa q^4 + \mu q^2 + 2\gamma\right)\right]. \quad (A.4)$$

The equation determining the Lagrange multiplier γ is

$$\alpha d^2 = \langle h^2 \rangle = \frac{\partial \omega}{\partial \gamma} = \frac{k_B T}{4\pi^2} \int \mathrm{d}^2 q \frac{1}{\kappa q^4 + \mu q^2 + \gamma}\cdot \quad (A.5)$$

The equation determining the surface tension σ is

$$\frac{A}{A_o} = \frac{\partial \omega}{\partial \mu} = 1 + \frac{1}{8\pi^2} \int \mathrm{d}^2 q \frac{q^2}{\kappa q^4 + \mu q^2 + \gamma}\cdot \quad (A.6)$$

Since exact integration in equations (A.4, A.6) is not possible, and since we are concerned mainly with the limit of small μ, we expand equations (A.4–A.6) in powers μ. In equations (A.4, A.5) we keep terms to order μ^2, which implies that in equation (A.6) we can keep only terms linear in μ to remain within the same order of accuracy. For ω this yields

$$\frac{\omega}{k_B T} \simeq \frac{\omega_o}{k_B T} + \frac{1}{4\sqrt{2}}\sqrt{\frac{\gamma}{\kappa}} + \left[\frac{1}{16\pi\kappa}\ln\left(\frac{\pi^4}{2a^4}\frac{\kappa}{\gamma}\right) + \frac{1}{k_B T}\right]\mu - \frac{\sqrt{2}\mu^2}{128\kappa^{3/2}\gamma^{1/2}}, \quad (A.7a)$$

where ω_o is the free-energy of a free membrane ($d \to \infty$) and is given by

$$\frac{\omega_o}{k_B T} = \frac{\pi}{8a^2}\ln\left(\frac{\pi a^2 \kappa}{2A_o k_B T}\right) - \frac{1}{4a^2}\cdot \quad (A.7b)$$

This constant will be omitted from now on, since it is not relevant for the quantities of interest. For d and A we get

$$\frac{\alpha d^2}{k_B T} = \frac{\langle h^2 \rangle}{k_B T} \simeq \frac{1}{8\sqrt{2\gamma\kappa}} - \frac{\mu}{16\pi\gamma\kappa} + \frac{\sqrt{2}}{256(\gamma\kappa)^{3/2}}\mu^2 \quad (A.7c)$$

$$\frac{A}{A_o} \simeq 1 + \frac{k_B T}{16\pi\kappa}\ln\left(\frac{\pi^4}{2a^4}\frac{\kappa}{\gamma}\right) - \frac{\sqrt{2}k_B T}{64k^{3/2}\gamma^{1/2}}\mu\cdot \quad (A.7d)$$

Solving equations (A.7c, A.7d) for γ and μ we find

$$\frac{\gamma(d,\mu)}{k_B T} \simeq \frac{k_B T}{128\kappa\alpha^2 d^4} - \frac{\mu}{8\pi\kappa\alpha d^2} - \frac{\mu^2}{4\kappa k_B T}\left(\frac{2}{\pi} - \frac{1}{2}\right) \quad (A.8)$$

and

$$\mu(A/A_o) \simeq -\frac{8\kappa}{\alpha d^2(1 - \frac{4}{\pi^2})}\left[\frac{A}{A_o} - \left(\frac{A}{A_o}\right)_{\mathrm{eq}}\right] \quad (A.9)$$

where we have defined

$$\left(\frac{A}{A_o}\right)_{\mathrm{eq}} = 1 + \frac{k_B T}{4\pi\kappa}\ln\left[\pi\sqrt{8\alpha}\left(\frac{\kappa}{k_B T}\right)^{1/2}\frac{d}{a}\right]\cdot \quad (A.10)$$

We are now able to perform a Legendre transform to obtain the Helmholtz free-energy per unit area, whose natural variables are d and A_o/A instead of γ and μ. This is defined according to

$$f = \left\{\left[\omega - \gamma\frac{\partial\omega}{\partial\gamma}\right]_{\gamma(d,\mu)} - \mu\frac{\partial\omega}{\partial\mu}\right\}_{\mu(A/A_o)} \quad (A.11)$$

where the subscripts of the brackets imply the use of equations (A.4, A.5) for $\gamma(d,\mu)$ and $\mu(A/A_o)$. This leads to

$$f = \frac{(k_B T)^2}{128\kappa\alpha d^2} + \nu\frac{\kappa}{d^2}\left[\frac{A}{A_o} - \left(\frac{A}{A_o}\right)_{\mathrm{eq}}\right]^2 \quad (A.12a)$$

where

$$\nu = \frac{3}{2(1 - 4/\pi^2)\alpha}\cdot \quad (A.12b)$$

From equation (A.12a) we see that a membrane near equilibrium behaves like an effective spring. Equation (A.12a) is identical to the result of Bruinsma and Rabin [11].

For a system at constant chemical potential the second term in equation (A.12a) is constant and one may calculate the corresponding compression modulus of the lamellar phase using $\bar{B} = d\ \partial^2 f/\partial d^2$ (see Appendix B). The result has to be compared [11] with the known expression due to Helfrich [37],

$$\bar{B} = \frac{9\pi^2}{64}\frac{(k_B T)^2}{\kappa d^3}\cdot \quad (A.13)$$

This implies that $\alpha = 1/3\pi^2$.

Appendix B: Generalized Landau-de-Gennes lamellar free-energy

The Helmhotlz free-energy of the whole lamellar phase is obtained by summing over the free-energies of the individual lamellae. Introducing the local variations of the interlayer spacing $\delta d(\mathbf{r})$ and of the physical projected area $\Delta(\mathbf{r})$, according to equations (13, 14b), leads to the free-energy given in equation (14a). It is also possible to obtain the free-energy in terms of the local variation of membrane volume fraction $\delta\phi(\mathbf{r})$ rather than $\Delta(\mathbf{r})$ [11,32]. Since

$$\phi = \frac{aA}{dA_{\rm o}} \tag{B.1}$$

we have, at *constant area* A,

$$\frac{\delta\phi}{\phi} + \frac{\delta d}{d} = -\frac{\delta A_{\rm o}}{A_{\rm o}} \equiv -\Delta. \tag{B.2}$$

Using this in equation (14a), collecting terms, and adding the Helfrich bending energy, we obtain the long wavelength generalized free-energy of the lamellar

$$F_{\rm lam} = \int {\rm d}^3 r \left[\frac{1}{2} K \left(\nabla_\perp^2 U \right)^2 + \frac{1}{2} B \left(\frac{\partial U}{\partial z} - \frac{1}{2} \left(\nabla_\perp U \right)^2 \right)^2 + \frac{1}{2} \chi^{-1} (\delta\phi)^2 + C_{\rm c} \left(\frac{\partial U}{\partial z} - \frac{1}{2} \left(\nabla_\perp U \right)^2 \right) \delta\phi \right] \tag{B.3a}$$

with the following values for the coefficients

$$B = \bar{B} + 2\mu \frac{\kappa}{d^3} \left[\left(\frac{A}{A_{\rm o}} \right)_{\rm eq} - \frac{k_{\rm B} T}{4\pi\kappa} \right]^2 \tag{B.3b}$$

$$\chi^{-1} = 2\mu \frac{\kappa}{d a^2} \tag{B.3c}$$

$$C_{\rm c} = 2\mu \frac{\kappa}{d^2 a} \left[\left(\frac{A}{A_{\rm o}} \right)_{\rm eq} - \frac{k_{\rm B} T}{4\pi\kappa} \right]. \tag{B.3d}$$

Upon minimizing equation (B.3a) over $\delta\phi$ we recover the familiar free-energy at constant chemical potential [13]

$$F_{\rm lam} = \int {\rm d}^3 r \left[\frac{1}{2} K \left(\nabla_\perp^2 U \right)^2 + \frac{1}{2} \bar{B} \left(\frac{\partial U}{\partial z} - \frac{1}{2} \left(\nabla_\perp U \right)^2 \right)^2 \right]. \tag{B.4}$$

The two moduli K and $\bar{B}$ define the well known smectic penetration length $\sqrt{K/B}$ [13].

Appendix C: Elliptic integrals

Here we express equations (35, 36) in terms of known elliptic integrals, as done by Singer [20]. This allows to use available asymptotic expansions for these known integrals to rederive equations (39, 42). Equation (36) is first expressed as [38]

$$D = \frac{2}{U_{\rm o}} \sqrt{\frac{\tilde{B}}{b}}\, t\, K\left[t\right] \tag{C.1}$$

where

$$t = \left(\frac{1}{Y} - 1 \right)^{-1/2} \; ; \; Y = \frac{b U_{\rm o}^2}{2a} \tag{C.2}$$

and where $K[k]$ is the complete elliptic integral of the first kind [38]

$$K[k] = \int_0^{\pi/2} \frac{{\rm d}\theta}{\sqrt{1 - k^2 \sin^2\,\theta}}\,. \tag{C.3}$$

Turning to equation (35) we find [38]

$$g_{\dot\gamma} = \left(\frac{1}{2} a U_{\rm o}^2 - \frac{1}{4} b U_{\rm o}^4 \right) D + \frac{2 U_{\rm o} a}{t} \sqrt{\frac{\tilde{B}}{b}} \left(E[t] - K[t] \right) + \frac{U_{\rm o} \sqrt{\tilde{B} b}}{3t} \left\{ \left(\frac{4a}{b} - U_{\rm o}^2 \right) K[t] - 4 \frac{a}{b} E[t] \right\} \tag{C.4}$$

where $E[k]$ is the complete elliptic integral of the second kind [38]

$$E[k] = \int_0^{\pi/2} {\rm d}\theta \sqrt{1 - k^2 \sin^2\,\theta}. \tag{C.5}$$

Using equation (C.1) to eliminate $K[t]$ in equation (C.4) we find

$$g_{\dot\gamma} = \frac{4}{3\sqrt{2}} \frac{\tilde{B}^{1/2} a^{3/2}}{b} \sqrt{1 - Y} E[t] + \frac{D a^2}{3b} \left(3Y - Y^2 - 2 \right). \tag{C.6}$$

The regime $\sigma \simeq \sigma_{\rm c}$ corresponds to $Y \ll 1$, and so to $t \ll 1$. Using asymptotic expansions for $E[t]$ and $K[t]$ for small t [38], we recover equation (39). The regime $\sigma \gg \sigma_{\rm c}$ corresponds to the bulk limit, $D \gg \xi$. Here we have $Y \simeq 1/2$ and $t \simeq 1$ and we immediately recover equation (42).

References

1. P.-G. de Gennes, *Scaling Concepts in Polymer Physics* (Cornell Uni., Ithaca, N.Y., 1979).
2. *Micelles, Membranes, Microemulsions and Monolayers*, edited by W.M. Gelbart, A. Ben-Shaul, D. Roux (Springer, N.Y., 1994).
3. S.A. Safran, *Statistical Thermodynamics of Surfaces, Interfaces, and Membranes*, Frontiers in Physics, Vol. 90 (Addison-Wesley, N.Y., 1994).
4. A. Onuki, J. Chem. Phys. **87**, 3692 (1987).
5. G.H. Fredrickson, J. Chem. Phys. **85**, 5306 (1986).
6. M.E. Cates, S.T. Milner, Phys. Rev. Lett. **62**, 182 (1989); C.M. Marques, M.E. Cates, J. Phys. France **51**, 1733 (1990).

7. H.F. Mahjoub, K.M. McGrath, M. Kleman, Langmuir **12**, 3131 (1996); H.F. Mahjoub, C. Bourgaux, P. Sergot, M. Kleman, Phys. Rev. Lett. **81**, 2076 (1998); O. Diat, D. Roux, Langmuir **11**, 1392 (1995).
8. P.D. Olmsted, C.-Y.D. Lu, Phys. Rev. E **56**, R55 (1997); P.D. Olmsted, P.M. Goldbart, Phys. Rev. A **46**, 4966 (1992).
9. G. Porte, J.-F. Berret, J.L. Harden, J. Phys. II France **7**, 459 (1997).
10. O. Diat, D. Roux, F. Nallet, J. Phys. II France **3**, 1427 (1993).
11. R. Bruinsma, Y. Rabin, Phys. Rev. A **45**, 994 (1992).
12. D. Sornette, N. Ostrowsky, Chap. 5 in reference [2].
13. P.-G. de-Gennes, J. Prost, *The Physics of Liquid Crystals* (Clarendon, Oxford, 1995), Sect. 7.1.7.
14. O. Diat, D. Roux, J. Phys. II France **3**, 9 (1993).
15. O. Diat, D. Roux, F. Nallet, Phys. Rev. E **51**, 3296 (1995).
16. D. Roux, F. Nallet, O. Diat, Europhys. Lett. **24**, 53 (1993).
17. O. Diat, thesis, Universite de Bordeaux I (1992).
18. J. Arrault, C. Grand, W.C.K. Poon, M.E. Cates, Europhys. Lett. **38**, 625 (1997).
19. P. Oswald, M. Kleman, J. Phys. Lett. France **43**, L411 (1983); P. Oswald, S.I. Ben-Abraham, J. Phys. France **43**, 1193 (1982).
20. S.J. Singer, Phys. Rev. E **48**, 2796 (1993).
21. The effect of shear flow on the single membrane undulations, with the velocity gradient within the lamellar planes, is discussed theoretically in: S. Ramaswamy, Phys. Rev. Lett. **69**, 112 (1992).
22. J. Yamamoto, H. Tanaka, Phys. Rev. Lett. **74**, 932 (1995).
23. D.R.M. Williams, F.C. MacKintosh, Macromolec. **27**, 7678 (1994).
24. J.M. Darlieu, J. Chem. Phys. **60**, 1081 (1974).
25. M. Delaye, R. Ribotta, G. Durand, Phys. Lett. A **44**, 139 (1973).
26. C.S. Rosenblatt, R. Pindak, N.A. Clark, R.B. Meyer, J. Phys. France **38**, 1105 (1977).
27. J.-i. Fukuda, A. Onuki, J. Phys. II France **5**, 1107 (1995).
28. E.I. Kats, V.V. Lebedev, Europhys. Lett. **22**, 469 (1993).
29. S. Ramaswamy, J. Prost, T.C. Lubensky, Europhys. Lett. **27**, 285 (1994).
30. D.J. Evans, H.J.M. Hanley, S. Hess, Phys. Today **37**, 26 (1984).
31. A finite permeation rate could make the response of the system be sensitive to the increment of increase, and to the rate of increase, of the shear rate. However, even in such situations we expect our assumption of zero permeation rate to be correct under certain conditions, for instance, when the shear rate increment (increase) is large. In this case the buckling texture develops fast and relaxes very slowly (*via* permeation), which makes our analysis useful.
32. T.C. Lubensky, J. Prost, S. Ramaswamy, J. Phys. France **51**, 933 (1990).
33. This constraint breaks the rotational invariance even in the absence of shear. This is because even a simple (virtual) rotation away from the initial orientation (parallel to the walls) implies streching of the membranes if the area of projection on the walls (the geometrical projected area) and the total membrane area in each layer are not allowed to change. Note however that simple rotation of the whole phase is in fact not allowed because of the boundary conditions $U(0) = U(D) = 0$.
34. It can be shown however that it always lies in the interval

$$\max\left[q_-\,,\left(\frac{\sigma}{6Kd}\right)^{1/2}\right] < q_{\rm c} < q_+$$

with

$$q_\pm^2 = \frac{\sigma}{2Kd}\left(1 \pm \sqrt{1-\frac{\sigma_{\rm c}^2}{\sigma^2}}\right).$$

Note that, for $\sigma \to \sigma_{\rm c}$, $q_\pm \to q_{\rm co}$ and so $q_{\rm c} \to q_{\rm co}$ too, as expected.
35. R. Messager, P. Bassereau, G. Porte, J. Phys. France **51**, 1329 (1990).
36. L. Golubovic, T.C. Lubensky, Phys. Rev. B **39**, 12110 (1989).
37. W. Helfrich, Z. Naturforsch **33a**, 305 (1978).
38. I.S. Gradshteyn, I.M. Ryzhik, *Tables of Integrals, Series, and Products* (Academic, London, 1980).